

# Single-arm three-wave interferometer for measuring dispersion of short lengths of fiber

Michael A. Galle, Waleed Mohammed, Li Qian and Peter W. E. Smith

Dept. of Electrical and Computer Engineering, University of Toronto  
10 King's College Road, Toronto, Ontario, Canada M5S 3G4  
[michael.galle@utoronto.ca](mailto:michael.galle@utoronto.ca), <http://www.ecf.utoronto.ca/~qianli>

**Abstract:** We present a simple fiber-based single-arm spectral interferometer to measure directly the second-order dispersion parameter of short lengths of fiber ( $< 50$  cm). The standard deviation of the measured dispersion on a 39.5-cm-long SMF28<sup>TM</sup> fiber is  $1 \times 10^{-4}$  ps/nm, corresponding to 1% relative error, without employing any curve fitting. Our technique measures the second-order dispersion by examining the *envelope* of the interference pattern produced by *three reflections*: two from the facets of the test fiber and one from a mirror placed away from the fiber facet at a distance that introduces the same group delay as the test fiber at the measured wavelength. The operational constraints on system parameters, such as required bandwidth, wavelength resolution, and fiber length, are discussed in detail. Experimental verification of this technique is carried out via comparison of measurements of single mode fiber (SMF28<sup>TM</sup>) with published data and via comparison of measurements of a dispersion compensating fiber with those taken using conventional techniques. Moreover, we used this new technique to measure the dispersion coefficient of a 45-cm-long twin-hole fiber over a 70 nm bandwidth. It is the first time dispersion measurement on this specialty fiber is reported.

©2007 Optical Society of America

**OCIS codes:** (120.3180) Interferometry; (060.2300) Fiber measurements; (260.2030) Dispersion

---

## References and links

1. J. H. Wiesenfeld and J. Stone, "Measurement of dispersion using short lengths of an optical fiber and picosecond pulses from semiconductor film lasers," *IEEE J. Lightwave Technol.* **2**, 464-468 (1984).
2. L. G. Cohen, "Comparison of single-mode fiber dispersion measurement techniques," *IEEE J. Lightwave Technol.* **3**, 958-966 (1985).
3. B. Costa, D. Mazzoni, M. Puleo, E. Vezzoni, "Phase shift technique for the measurement of chromatic dispersion in optical fibers using LEDs," *IEEE Trans. Microwave Theory Tech.* **82**, 1497-1503 (1982).
4. Agilent White Paper, "Agilent 86038B photonic dispersion and loss analyzer," (2007) <http://cp.literature.agilent.com/litweb/pdf/5989-2325EN.pdf>
5. L. Cherbi, M. Mehenni, and R. Aksas, "Experimental investigation of the modulation phase-shift method for the measure of the chromatic dispersion in a single-mode fiber coiled on a cover spool," *Microw. Opt. Technol. Lett.* **48**, 174-178 (2006).
6. P. Merrit, R. P. Tatam, and D.A. Jackson, "Interferometric chromatic dispersion measurements on short lengths of monomode optical fiber," *IEEE J. Lightwave Technol.* **7**, 703-716 (1989).
7. R. Cella and W. Wood, "Measurement of chromatic dispersion in erbium doped fiber using low coherence interferometry," in *Proceedings of the Sixth Optical Fiber Measurement Conference (OFMC'01)*, 207-210 (2001).
8. J. Gehler and W. Spahn, "Dispersion measurement of arrayed-waveguide grating by Fourier transform spectroscopy," *Electron. Lett.* **36**, 338-340 (2000).
9. C. Palavicini, Y. Jaouën, G. Debarge, E. Kerrinckx, Y. Quiquempois, M. Douay, C. Lepers, A.-F. Obaton, G. Melin, "Phase-sensitive optical low-coherence reflectometry technique applied to the characterization of photonic crystal fiber properties," *Optics Letts.* **30**, 361-363 (2005).

10. A. Wax, C. Yang, and J. A. Izatt, "Fourier-domain low-coherence interferometry for light-scattering spectroscopy," *Opt. Lett.* **28**, 1230-1232 (2003).
11. R. K. Hickernell, T. Kazumasa, M. Yamada, M. Shimizu, M. Horiguchi. "Pump-induced dispersion of erbium-doped fiber measured by Fourier-transform spectroscopy", *Opt. Lett.* **18**, 19-21 (1993).
12. P. Hlubina, "White-light spectral interferometry to measure intermodal dispersion in two-mode elliptical core optical fibers", *Opt. Commun.* **218**, 283-289 (2003).
13. P. Hlubina, T. Martynkien, and W. Urbanczyk, "Dispersion of group and phase modal birefringence in elliptical-core fiber measured by white-light spectral interferometry," *Opt. Express* **11**, 2793-2798 (2003).
14. J. Tignon, M. V Marquezini, T. Hasch, and D. S. Chemals, "Spectral interferometry of semiconductor nanostructures," *IEEE J. Quantum Electron.* **35**, 510-522 (1999).
15. C. D. Dorrer, N. Belabas, J. P. Likforman, and M. Joffre, "Spectral resolution and sampling in Fourier transform spectral interferometry," *J. Opt. Soc. Am. B* **17**, 1795-1802 (2000).
16. J. Y. Lee and D. Y. Kim, "Versatile chromatic dispersion measurement of a single mode fiber using spectral white light interferometry," *Opt. Express* **14**, 11608-11615 (2006).
17. P. Hlubina, M. Szpulak, D. Ciprian, T. Martynkien and W. Urbanczyk, "Measurement of the group dispersion of the fundamental mode of holey fiber by white-light spectral interferometry," *Opt. Express* **15**, 11073-11081 (2006).
18. A. B. Vakhtin, K. A. Peterson, W. R. Wood, and D. J. Kane, "Differential spectral interferometry and imaging technique for biomedical applications," *Opt. Lett.* **28**, 1332-1334 (2003).
19. R. Leitgeb, W. Drexler, A. Unterhuber, B. Hermann, T. Bajraszewski, T. Le, A. Stingl, and A. Fercher, "Ultra high resolution Fourier domain optical coherence tomography," *Opt. Express* **12**, 2156-2165 (2004).
20. D. Huang, E. A. Swang, C. P. Lin, J. S. Schuman, W. G. Stinson, W. Chang, M. R. Hee, T. Flotte, K. Gregory, C. A. Puliafito, and J. G. Fugimoto, "Optical coherence tomography," *Science* **254**, 1178-1181 (1991).
21. M. Wojtkowski, R. Leitgeb, A. Kowalczyk, T. Bajraszewski, and A. F. Fercher, "In vivo human retinal imaging by Fourier domain optical coherence tomography," *J. Biomed. Opt.* **7**, 457-463 (2002).
22. M. Wojtkowski, A. Kowalczyk, R. Leitgeb, and A. F. Fercher, "Full range complex spectral optical coherence tomography technique in eye imaging," *Opt. Lett.* **27**, 1415-1417 (2002).
23. G. Hausler and M. W. Lindner, "Coherence radar and spectral radar – new tools for dermatological diagnosis," *J. Biomed. Opt.* **3**, 21-31 (1998).
24. A. F. Fercher, C. K. Hitzenberger, G. Kamp, and S. Y. Elzaiat, "Measurement of intraocular distances by backscattering spectral interferometry," *Opt. Commun.* **117**, 43-48 (1995).
25. Andrei B. Vakhtin, Daniel J. Kane, William R. Wood, and Kirsten A. Peterson. "Common-path interferometer for frequency-domain optical coherence tomography," *Appl. Opt.* **42**, 6953-6958 (2003).
26. U. Sharma, N. M. Fried, J. U. Kang, "All-fiber common-path optical coherence tomography: sensitivity optimization and system analysis," *IEEE J. Sel. Top. Quantum Electron.* **11**, 799-805 (2005).
27. Corning Inc., "Corning SMF-28™ optical fiber product information", PI1036, (2002) [www.corning.com/opticalfiber](http://www.corning.com/opticalfiber)
28. P. Blazkiewicz, W. Xu, D. Wong, S. Fleming, and T. Ryan, "Modification of thermal poling evolution using novel twin-hole fibers," *IEEE J. Lightwave Technol.* **19**, 1149-1154 (2001).
29. P. G. Kazansky, L. Dong, and P. S. J. Russell, "High second-order nonlinearities in poled silicate fibers," *Opt. Lett.* **19**, 701-703 (1994).
30. M. Fokine, L. E. Nilsson, Å. Claesson, D. Berlemont, L. Kjellberg, L. Krummenacher, and W. Margulis, "Integrated fiber Mach-Zehnder interferometer for electro-optic switching," *Opt. Lett.* **27**, 1643-1645 (2002).

---

## 1. Introduction

Dispersion is a critical parameter in the design of high-speed photonic systems since it affects the system bandwidth via pulse broadening. Dispersion engineering is also widely used in ultrafast optical systems. Two of the most widely used commercial dispersion measurement techniques are the time of flight (TOF) technique [1] and the Modulation Phase Shift (MPS) technique [2, 3]. In the TOF technique, the second-order dispersion parameter, hereafter referred to simply as dispersion, is determined by measuring the relative temporal delay between pulses at different wavelengths. In the MPS technique, an optical signal is amplitude modulated by an RF signal and the dispersion parameter is determined by measuring the RF phase delay experienced by the optical carriers at the different wavelengths. Measurement precision achievable by the TOF and MPS techniques are on the order of 1 ps/nm [2] and 0.07

ps/nm [4], respectively. Due to its higher precision, MPS has become the industry standard method for measuring dispersion in optical fibers. However, MPS is expensive to implement and its precision is limited by both the stability and the jitter in the RF signal [5]. Moreover, both the TOF and the MPS techniques require long lengths of fiber, from several tens of meters to several kilometers. Therefore, they are not desirable for characterizing specialty fibers or gain fibers, of which large fiber lengths are expensive to acquire or not available. Also, when fiber uniformity changes significantly along its length, the dispersion of a long span of fiber cannot be used to accurately represent that of a short section of fiber. In such cases, dispersion measurement performed directly on short fiber samples is desirable.

Interferometric techniques, on the other hand, are capable of measuring dispersion on fibers of length below 1m [6]. There are two categories of interferometric techniques: temporal and spectral. Temporal interferometry [7-11] employs a broadband source and a variable optical path to produce a temporal interferogram between a fixed path through the test fiber and the variable path. The spectral amplitude and phase are then determined from the Fourier transform of the temporal interferogram. The dispersion is indirectly obtained by taking the derivative of the spectral phase. A precision of 0.0015 ps/nm measured on a 0.814-m-long photonic crystal fiber [9] was recently reported using temporal interferometry. The main disadvantage of temporal interferometry is that it is susceptible to noise resulting from both translation inaccuracy and vibration of the optics in the variable path. A tracking laser is typically required to calibrate the delay path length [8, 9].

Spectral interferometry is generally more stable since the arms of the interferometer are kept stationary, and no tracking laser is necessary. It is often chosen for the dispersion characterization of photonic components [12-17] and depth-resolved optical imaging [18] such as optical coherence tomography (OCT) [19-24]. In spectral interferometry, spectral fringes are produced by the interference of broadband light after propagating through two paths: one contains the test fiber and the other is a reference path containing a fixed delay. The spectral phase of the lightwave passing through the test fiber relative to that through the reference path can be extracted from the fringe pattern, and in principle, higher order dispersion can be derived. Though accurate results on group delay, dispersion, and dispersion slope have been reported using this indirect method [16], the requirement on raw measurement accuracy is high and a number of curve fittings and data processing steps are required to obtain higher order dispersions, which may affect the accuracy of the results. In contrast, it is also possible to measure the second-order dispersion directly by employing a *balanced* dual-arm interferometer [6] with an adjustable optical path in one arm. The adjustable arm is adjusted to have the same group delay as the test fiber to remove the effect of the large linear dispersion in the interferogram. A precision of 0.00007 ps/nm has been reported on a SMF of 1m using this technique [6].

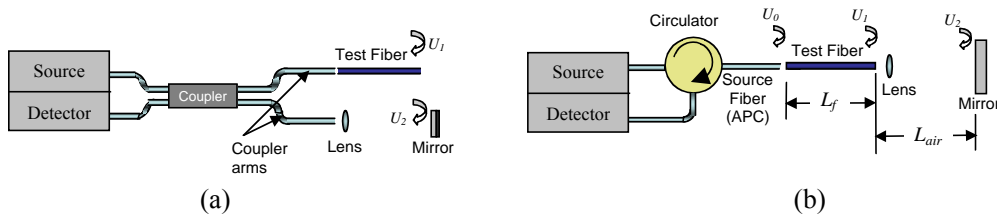


Fig. 1. (a) General dual-arm balanced Michelson interferometer. The spectral interferogram is produced by two reflected waves  $U_1$  and  $U_2$ . (b) Single-arm interferometer where the spectral interferogram is produced by three reflected waves;  $U_0$ ,  $U_1$  and  $U_2$ .

The balanced dual-arm interferometers are typically in a Mach-Zehnder or a Michelson configuration. In the balanced Michelson interferometer set up (Fig. 1(a)), a spectral interferogram is created from the reflections of the two paths  $U_1$  and  $U_2$ , as shown. One drawback of the fiber-based dual-arm configuration is that the optical path lengths of the two

fiber leads coming out of the coupler ideally need to be exactly the same; otherwise an extra set of interference fringes is created by the reflections from the two end facets of the coupler fiber leads, which distorts the spectral interferogram. Alternatively and more practically, the two leads are intentionally made to have a large length difference so that the undesirable fringes are “fast” varying and can be eliminated by a low-resolution spectrometer. In the latter case, the dispersion of the coupler fiber will be added to that of the test fiber, and therefore the former must be calibrated precisely.

In this paper we introduce an alternative and simpler method, the Single-Arm Interferometer (SAI) as shown in Fig. 1(b), for the direct measurement of dispersion in short fibers. This not only is a much simpler configuration, it also eliminates the need to calibrate the dispersion of the fibers in the measurement system (assuming the dispersion introduced by the collimating lens is negligible). Its simpler construction also makes it less susceptible to polarization and phase instabilities. Like the balanced Michelson interferometer, the SAI is also balanced since the free space path is adjusted to cancel the group delay of the test fiber, and both the second- and third-order dispersions can be obtained directly. The conceptual difference between the two techniques is that, in the SAI, the interference pattern is produced by *three* waves: two from the reflections at the facets of the test fiber and one from a mirror placed behind it (as shown by  $U_o$ ,  $U_1$ , and  $U_2$  in Fig. 1(b)). The beating between the interference fringes produced by the test fiber and those by the air path generates an *envelope* which is equivalent to the interference pattern produced by two waves ( $U_1$  and  $U_2$  in Fig. 1(a)) in a dual-arm interferometer.

The SAI configuration appears similar to common-path interferometers, often used for depth imaging as in Common-Path Optical Coherence Tomography (CP-OCT) [25, 26]. It is, however, fundamentally different from CP-OCT since it utilizes 3 reflections, and extracts the *dispersion* parameters directly from the *envelope* of the interference pattern. In the next section, we will briefly present the theoretical representation of the interference pattern, the phase between the adjacent peaks/troughs of the envelope, and its relationship to the dispersion.

## 2. Theory

In a SAI, the dispersion parameter is obtained from the *envelope* of the interference pattern generated by three waves  $U_o$ ,  $U_1$  and  $U_2$  as depicted in Fig. 1(b). The amplitudes of  $U_o$  and  $U_1$  are in general proportional to the Fresnel reflection coefficients for a glass-air interface. The amplitude of  $U_2$  depends on the amount of light coupled back to the fiber.  $U_1$  and  $U_2$  can be expressed relative to  $U_o$  in amplitude and in phase by:

$$\begin{aligned} U_1 &= \alpha U_o e^{-j2\beta L_f} \\ U_2 &= \gamma U_o e^{-j2\beta L_f - j2k_o L_{air}} \end{aligned} \quad (1)$$

In (1)  $L_f$  and  $L_{air}$  are the lengths of the test fiber and the air path, respectively.  $\beta$  and  $k_o$  are, respectively, the propagation constant of the fundamental mode in fiber, and the propagation constant in free space.  $\alpha$  and  $\gamma$  are the relative field amplitudes with respect to  $U_o$ .

The intensity interference pattern produced by the superposition of  $U_o$ ,  $U_1$  and  $U_2$  is represented by:

$$\begin{aligned} I_o &= |U_o + U_1 + U_2|^2 = U_o^2 \left| 1 + \alpha e^{-i2\beta L_f} + \gamma e^{-i2\beta L_f - i2k_o L_{air}} \right|^2 \\ &= U_o^2 \left\{ 1 + \alpha^2 + \gamma^2 - 2\alpha\gamma \cos^2(\beta L_f + k_o L_{air}) + 2\alpha(1 - \gamma) \cos(2\beta L_f) \right. \\ &\quad \left. + 4\alpha\gamma \cos(\beta L_f + k_o L_{air}) \cos(\beta L_f - k_o L_{air}) \right\} \end{aligned} \quad (2)$$

The expression in (2) can be treated as a fast-varying “carrier” (with respect to frequency or wavelength) modified by an upper and a lower slow-varying envelope, as shown in Fig. 2 (left), which depicts the simulated spectral interferogram generated by the 3-wave SAI with a 30-cm SMF28 fiber as the test fiber. Upon closer examination (Fig. 2, lower right), the

“carrier” is not a pure sinusoidal function, because there are three fast-varying phases in (2),  $2(\beta L_f + k_o L_{air})$ ,  $(\beta L_f + k_o L_{air})$ , and  $2\beta L_f$ , all of which vary much faster than the phase of the envelope ( $\phi_{envelope}$ ), which equals  $\beta L_f - k_o L_{air}$ . When  $\gamma$  is large ( $>0.5$ ), it can be shown that the upper envelope is approximated by

$$I_{upper\_env} \approx U_o^2 \left( 1 + \alpha^2 + \gamma^2 + 2\alpha(\gamma - 1) + 2\gamma + 4\alpha \left| \cos(\phi_{envelope}) \right| \right) \quad (3)$$

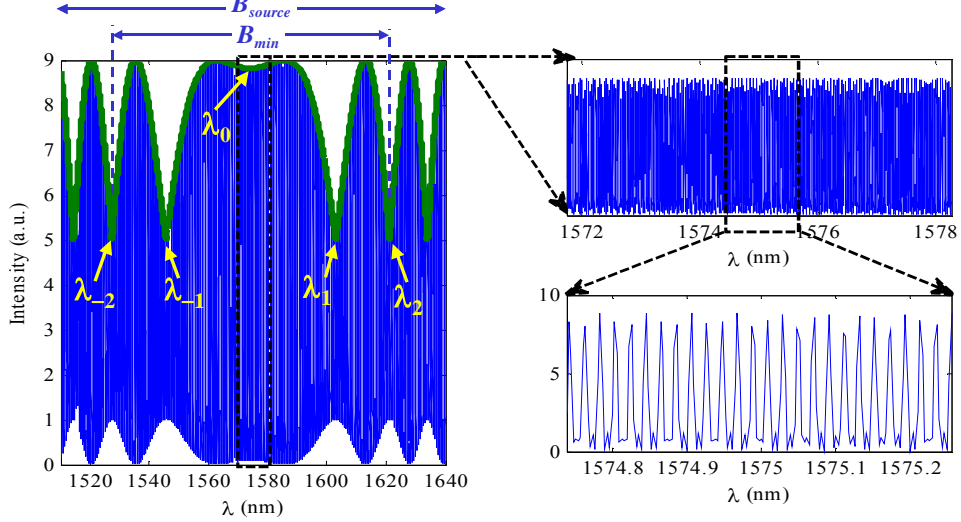


Fig. 2. Simulated spectral interferogram produced by the setup in Fig. 1(b) for a 30-cm-long SMF28<sup>TM</sup> as the test fiber, with  $\alpha = \gamma = 1$ . The parameters used for the SMF28<sup>TM</sup> fiber are given in [27]. The thick green line represents the function calculated by Eq. (3), which is a close approximation of the upper envelope.  $B_{min}$  denotes the minimum required bandwidth, and  $B_{source}$  is the source bandwidth, which determines the extent of the interferogram.  $\lambda_0$  is the balanced wavelength.  $\lambda_1$  and  $\lambda_2$  are wavelengths corresponding to two adjacent troughs on one side of  $\lambda_0$ .

The envelope function expressed by (3) is plotted in Fig. 2 in green, which is a good approximation of the actual envelope of the carrier. Replacing  $\beta$  with  $2\pi n_{eff}/\lambda$ , where  $n_{eff}$  is the effective index of the fiber, and applying Taylor expansion to  $n_{eff}$ , we can obtain the following expression for  $\phi_{envelope}$  [6]:

$$\begin{aligned} \phi_{envelope}(\lambda) = 2\pi \left\{ \frac{1}{\lambda} \left[ \left( n_{eff}(\lambda_o) - \lambda_o \frac{dn_{eff}}{d\lambda} \Big|_{\lambda_o} \right) L_f - L_{air} \right] + L_f \frac{dn_{eff}}{d\lambda} \Big|_{\lambda_o} \right. \\ \left. + L_f \frac{(\lambda - \lambda_o)^2}{2! \lambda} \frac{d^2 n_{eff}}{d\lambda^2} \Big|_{\lambda_o} + L_f \frac{(\lambda - \lambda_o)^3}{3! \lambda} \frac{d^3 n_{eff}}{d\lambda^3} \Big|_{\lambda_o} + \dots \right\} \quad (4) \end{aligned}$$

The first term in (4) (in square brackets) disappears when  $L_{air}$  is adjusted to balance out the group delay of the test fiber at  $\lambda_o$ .  $\lambda_o$  is herein referred to as the balanced wavelength. The envelope phase difference at two separate wavelengths,  $\lambda_1$  and  $\lambda_2$ , that correspond to two peaks (or two troughs) of the envelope is :

$$\begin{aligned} \Delta \phi_{envelope} &= \left| \phi_{envelope}(\lambda_2) - \phi_{envelope}(\lambda_1) \right| \\ &= 2\pi \left( \left[ \frac{(\lambda_2 - \lambda_o)^2}{2! \lambda_2} - \frac{(\lambda_1 - \lambda_o)^2}{2! \lambda_1} \right] \frac{d^2 n_{eff}}{d\lambda^2} \Big|_{\lambda_o} + \left[ \frac{(\lambda_2 - \lambda_o)^3}{3! \lambda_2} - \frac{(\lambda_1 - \lambda_o)^3}{3! \lambda_1} \right] \frac{d^3 n_{eff}}{d\lambda^3} \Big|_{\lambda_o} \right) L_f \quad (5) \\ &= m\pi \end{aligned}$$

Note that  $m$  is the number of fringes between the two wavelengths. If this phase difference is taken using two pairs of peaks/troughs (e.g.,  $\lambda_1$  &  $\lambda_2$ , and  $\lambda_{-1}$  &  $\lambda_{-2}$ ), the result is a system of equations in which  $\left. \frac{d^2 n_{eff}}{d\lambda^2} \right|_{\lambda_o}$  and  $\left. \frac{d^3 n_{eff}}{d\lambda^3} \right|_{\lambda_o}$  can be solved directly [6]. Note that, if

we ignore the third-order dispersion, then only one pair of wavelengths (e.g.,  $\lambda_1$  &  $\lambda_2$ ) is required to calculate the second-order dispersion, however, it would be less accurate. The dispersion parameter  $D$  can then be found as follows:

$$D(\lambda_o) = -\frac{\lambda_o}{c} \left. \frac{d^2 n_{eff}}{d\lambda^2} \right|_{\lambda_o} \quad (6)$$

We remark that the birefringence in the test fiber will affect the polarization states of the two reflected waves and therefore will affect fringe visibility. This effect is typically small for weakly birefringent fiber since the length of the test fiber is small, and a polarization controller is not necessary. (Note, the measured dispersion does not depend on fringe visibility, though a high visibility will allow a more accurate determination of the peak/trough wavelengths.) In the case of a strongly birefringent test fiber, a polarization controller can be placed before the input port of the circulator (Fig. 1(b)) to make the input polarization to the test fiber one of its principal states of polarization, and fringe visibility can be maximized. In principle, this technique can also be used to determine the dispersion parameters for the two polarization modes of the fiber.

The main difference between the interferogram produced in this setup and those produced by balanced dual-arm interferometers is the presence of the fast “carrier”. In the case of a balanced dual-arm interferometer, the dispersion is calculated from the interference pattern, whereas here the dispersion is calculated from the envelope of the interference pattern. The advantage of our scheme is that only a single arm is sufficient, and there is no need for calibration.

### 3. Constraints on system parameters

In this section, we discuss the constraints on several important system parameters: wavelength resolution of the measurement, minimum required bandwidth of the source, measurable bandwidth of the dispersion curve, and the test fiber length. The relationships between these parameters are derived and discussed.

#### 3.1 Wavelength resolution of dispersion measurement

It is important to note that the wavelength resolution of the instrument (e.g., the step size of the tunable laser) is not the wavelength resolution of the measured dispersion curve. The former is related to the spectral resolution of the interferogram, from which only one dispersion value (at the balanced wavelength) can be obtained. The latter is related to the minimum step size of the mirror translation. This is because variation of the air path changes the balanced wavelength ( $\lambda_o$ ). The relationship between the air path length  $L_{air}$  and the fiber length  $L_f$  at  $\lambda_o$  is given by:

$$L_{air} = \left( n_{eff}(\lambda_o) - \lambda_o \left. \frac{dn_{eff}}{d\lambda} \right|_{\lambda_o} \right) L_f \quad (7)$$

Taking the derivative of  $L_{air}$  with respect to  $\lambda_o$  and using the definition given by (6), we obtain

$$\left. \frac{dL_{air}}{d\lambda} \right|_{\lambda_o} = \left( -\lambda_o \left. \frac{d^2 n_{eff}}{d\lambda^2} \right|_{\lambda_o} \right) L_f = cD(\lambda_o)L_f \quad (8)$$

From (8), the relationship between a change in the balanced wavelength,  $\delta\lambda_o$ , and the change in the air path length,  $\delta L_{air}$ , is given by:

$$\delta\lambda_o = \frac{\delta L_{air}}{cL_f D} \quad (9)$$

Thus the minimum step size of the air path sets the wavelength resolution of the measured dispersion curve. Note the wavelength resolution is also inversely proportional to the dispersion-length product of the test fiber. We will later show that many other system parameters are dependent on this product. As a numerical example, for a step size of  $0.1\mu\text{m}$ , assuming a 50-cm-long SMF28<sup>TM</sup> test fiber, the wavelength resolution is  $0.1\text{nm}$ , which is sufficient for most applications. Note also that the sign of the dispersion can be determined by varying the air path length and observing the change in the balanced wavelength. From (9), a negative dispersion value should result in an increase in the balanced wavelength for a decrease in the air path length.

### 3.2 Minimum required source bandwidth ( $B_{min}$ )

A minimum number of *envelope* fringes is required for accurate measurements of dispersion. From Section 2, as long as the balanced wavelength ( $\lambda_0$ ) and four other wavelengths corresponding to the peaks (or troughs) of the envelope fringes are captured within the source bandwidth,  $B_{source}$ , (see Fig. 2), one can determine the dispersion  $D(\lambda_0)$ . It is found in practice that more accurate measurements require selecting two peaks (or troughs) on either side of  $\lambda_0$ , as indicated by  $B_{min}$  on Fig. 2.

For a given test fiber, the dispersion-length product is fixed. Therefore, the only factor that limits the number of *envelope* fringes is the source bandwidth,  $B_{source}$ . The longer the fiber, or the larger the dispersion, the more closely spaced the envelope fringes, and hence the smaller the required bandwidth. In order to determine  $B_{min}$  quantitatively, we need to determine the maximum value for the wavelength spacing ( $\lambda_2 - \lambda_0$ ), as shown in Fig. 2. From (4), ignoring the 3<sup>rd</sup>-order term, we can obtain the envelope phase difference  $|\phi_{envelope}(\lambda_1) - \phi_{envelope}(\lambda_0)|$ , which has an upper bound of  $\pi$ , since the first trough occurs at  $\lambda_1$ :

$$|\phi_{envelope}(\lambda_1) - \phi_{envelope}(\lambda_0)| = 2\pi \frac{(\lambda_1 - \lambda_0)^2}{2! \lambda_1} \frac{d^2 n_{eff}}{d\lambda^2} \Big|_{\lambda_0} L_f \leq \pi \quad (10)$$

Applying the definition of dispersion in (6), we can therefore find the upper bound of the wavelength spacing ( $\lambda_1 - \lambda_0$ ):

$$\lambda_1 - \lambda_0 \leq \frac{\lambda_0}{\sqrt{cDL_f}} \quad (11)$$

Next, we examine the wavelength spacing between  $\lambda_1$  and  $\lambda_2$ . From (5), ignoring the 3<sup>rd</sup>-order term and applying (6), we get,

$$(\lambda_2 - \lambda_0)^2 - (\lambda_1 - \lambda_0)^2 \approx \frac{\lambda_0^2}{cDL_f} \quad (12)$$

Combining Eq (11) and (12), we get the upper bound for the wavelength spacing  $\lambda_2 - \lambda_0$ :

$$(\lambda_2 - \lambda_0)^2 = [(\lambda_2 - \lambda_1) + (\lambda_1 - \lambda_0)]^2 \leq \frac{2\lambda_0^2}{cDL_f} \quad (13)$$

and the minimum required source bandwidth  $B_{min}$  should be not less than the upper bound of  $2(\lambda_2 - \lambda_0)$ , i.e.,

$$B_{min} = 2\sqrt{2} \frac{\lambda_0}{\sqrt{cDL_f}} \quad (14)$$

It is clear that the dispersion-length product of the test fiber also affects the minimum required bandwidth. Using a similar numerical example, assuming a 50-cm-long SMF test fiber and 1.55 $\mu\text{m}$  as the balanced wavelength, the minimum required bandwidth is 85 nm.

### 3.3 Measurable bandwidth of the dispersion curve $B_{mea}$

Since each spectral interferogram produces one dispersion value at the balanced wavelength,  $\lambda_0$ , to obtain dispersion versus wavelength, a number of interferograms are recorded at various balanced wavelengths by setting the appropriate air path lengths. Since each interferogram should be taken over a bandwidth of at least  $B_{min}$ , from Fig. 3, one can see that the measurable bandwidth of the dispersion curve is the difference between the available source bandwidth  $B_{source}$  and the minimum required bandwidth  $B_{min}$ , that is,

$$B_{mea} = B_{source} - B_{min} \geq B_{source} - 2\sqrt{2} \frac{\lambda_0}{\sqrt{cDL_f}} \quad (15)$$

Alternatively, if we do not require two of the troughs to be on each side of  $\lambda_0$ , then the measurable bandwidth  $B_{mea}$  can be larger. In order to accurately determine  $\lambda_0$ , we would still need the central fringe (from  $\lambda_{-1}$  to  $\lambda_1$  in Fig. 2) to be entirely visible within the measured spectral range. Therefore,

$$B_{mea} = B_{source} - 2(\lambda_1 - \lambda_0) \geq B_{source} - 2 \frac{\lambda_0}{\sqrt{cDL_f}} \quad (16)$$

Eq (15) or (16) gives the lower bound for the measurable bandwidth, which assumes the widest possible central fringe. In practice, since  $\phi_{envelope}(\lambda_0)$  cannot be controlled, the width of the central fringe can be anywhere between zero and twice the limit of (11). Therefore,  $B_{mea}$  can be as large as  $B_{source}$  in certain cases.

Examination of (15) or (16) shows that increasing the dispersion-length product of the test fiber increases  $B_{mea}$ . Note that for a given measurement system,  $B_{source}$  is fixed, so the only parameter that can be used to extend  $B_{mea}$  is  $L_f$ . The next section discusses the range of fiber lengths that can be measured using the SAI technique.

Fig. 3 summarizes the dependence of wavelength resolution, the minimum required bandwidth, and the measurable bandwidth on the dispersion-length product of the test fiber.

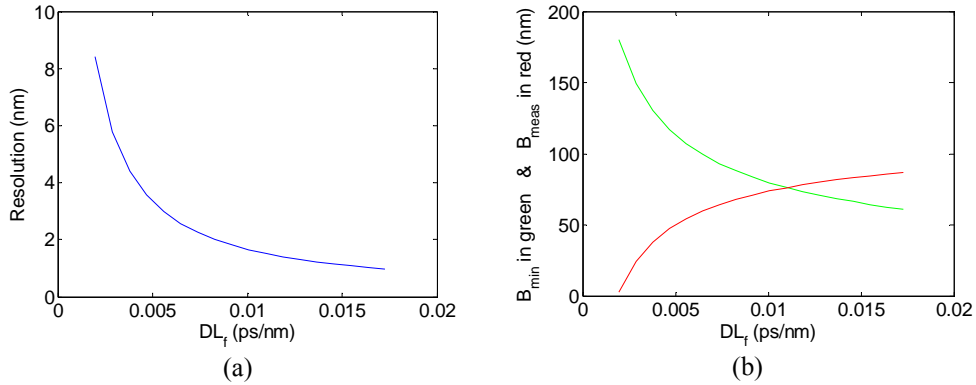


Fig. 3: (a) The dependence of wavelength resolution on the dispersion-length product ( $DL_f$ ). (b) The dependence of the minimum required bandwidth ( $B_{min}$ ) and the measurable bandwidth ( $B_{mea}$ ), on the  $DL_f$  product. Note we assume the values  $\lambda_0 = 1550\text{nm}$  and  $\delta L_{air} = 5\mu\text{m}$  and  $B_{source} = 130\text{nm}$  for these figures.

### 3.4 Minimum fiber length

The bandwidth of the source limits the minimum fiber length, since if the fiber length is too small, the spectral interferogram will not contain sufficient envelope fringes for an accurate dispersion measurement. Thus the requirement is that:

$$B_{\min} \leq B_{\text{source}} \quad (16)$$

Using (15), we have:

$$L_f \geq \frac{8\lambda_o^2}{cDB_{\text{source}}^2} \quad (17)$$

Note that for a longer fiber there will be a greater measurement bandwidth (according to (15) or (16)) and a higher wavelength resolution (9). As a numerical example, for a source bandwidth of 130nm, the minimum length for a SMF28<sup>TM</sup> fiber is 0.23m.

### 3.5 Maximum fiber length

The SAI method uses the slow-varying envelope function to obtain dispersion. Though the “carrier” fringes are not of interest, they still need to be resolved during measurement, otherwise the envelope shape cannot be preserved. The carrier fringe spacing is directly affected by the length of the fiber under test,  $L_f$ . A longer fiber will lead to narrower carrier fringes. From (2), it can be seen that, though the carrier is not a pure sinusoidal function, its fast-varying phase is approximately periodic, with a period that is on the order of  $\lambda_o^2/2n_{\text{eff}}L_f$ . If we apply the Nyquist sampling criterion and assume that at least 2 sample points have to be included in one fringe, then the maximum limit on the fiber length becomes:

$$L_f \leq \frac{\lambda_o^2}{4n_{\text{eff}} \Delta\lambda} \quad (18)$$

where  $\Delta\lambda$  is the wavelength resolution of the measurement system (or, to be more specific, the wavelength step size of the tunable laser). If the fiber length limit is exceeded, aliasing occurs.

The preceding analysis assumes that the interferogram is sampled without aliasing (within the Nyquist limit). It is useful to point out, since we are interested only in the *envelope* of the interferogram, it is possible to use fiber lengths exceeding the limit given in (18). For a sufficiently long test fiber, many carrier fringes can appear within a small wavelength window over which the envelope function remains relatively constant. When operating beyond the Nyquist limit, it is possible and probable that one or more of the carrier fringe peaks are sampled (given a certain tolerance) within the wavelength window, even though not all of the peaks are captured. Therefore, by taking only one maximum value within every wavelength window, one will be able to obtain an accurate representation of the *envelope* of the interferogram, even if the interferogram itself is not sampled adequately. Though it is possible (but not probable) that the wavelength step of the measurement is an exact integer multiple of the carrier period, and none of the carrier fringe peaks is captured, this “unlucky” situation can be prevented by using a non-uniform wavelength step size. For example, one can use random step sizes that has a distribution (e.g., a Gaussian distribution) about an average value. In practice, the instrument’s inherent inaccuracy in wavelength sweeping usually provides the required randomness of the wavelength step size, and test fiber length can well exceed the limit set in (18). For example, if the step sizes exhibit a Gaussian distribution with a mean of 1 pm and a standard deviation of 1 pm, then a detailed statistical analysis (not shown here for the purpose of brevity) shows that the probability of sampling at least one carrier peak within a 0.25 nm window is greater than 99% regardless of fiber length. Here, “capturing” a peak means a sample is taken within a region of  $\pm 1\%$  of the carrier period, centered on the carrier peak. Ultimately, the test fiber length is limited by the laser linewidth (which can be much smaller than the carrier fringe period) and the maximum air path length.

#### 4. Experimental results and analysis

The experimental set up is shown in Fig. 1(b). The tunable laser source (Agilent 81640A) and detector (Agilent 81632A) used are plug-in modules of the Agilent 8164A Lightwave Measurement System. The source has a linewidth of 100KHz, a tuning range of 130 nm centered around 1550 nm, and a minimum *average* wavelength step of 1 pm (with a standard deviation 0.17 pm). The unit records the detector readings and the wavelength readings as the source wavelength is swept. Currently, due to the limited onboard memory of the detector module, data transfer between the module and the computer is required every 1 nm of scan, which results in a very long measurement time (about 10 minutes) for obtaining one spectral interferogram over the entire tuning range. With sufficient memory in newer modules, the measurement time can be shortened to be within a few seconds, since step accuracy is not required (and indeed should be avoided, see Section 3.5) during scan. An angle-polished connector is used at the launch fiber as shown in Fig. 1(b) in order to eliminate the reflection from this facet. The reflections from the collimation lens surfaces are suppressed by using an antireflection coated lens. The dispersion of the lens is negligible. The mirror tilt is adjusted to obtain maximum fringe visibility. The mirror translation is controlled manually, and the minimum step is approximately 5 $\mu$ m.

In the following sections, we will apply the SAI technique to measure the dispersion of three different fibers: a standard SMF28<sup>TM</sup> single mode fiber, a Dispersion Compensating Fiber (DCF) and a Twin-Hole Fiber (THF). In measuring the envelope of the spectral interferogram, the total scanning region is divided into 0.25-nm-wide wavelength bands, over which the envelope is considered constant. The peak value within each band is extracted to produce the spectral envelope.

##### 4.1 Corning SMF28<sup>TM</sup>

The dispersion properties of SMF28<sup>TM</sup> are well known and hence it was used to verify the SAI technique. In this experiment we used a 39.5-cm piece of the SMF28<sup>TM</sup> fiber, and the result is shown in Fig. 4. The wavelength resolution of the measured dispersion curve, as determined by (9), is 2.4 nm. The measurable bandwidth according to (15) is 30 nm, which is the bandwidth actually used, as shown in Fig. 4(b). The standard deviation of the measurement results is calculated from their deviations to the linear fit of the measured dispersion values. This is justified as the dispersion slope can be treated as constant within the 30-nm bandwidth (i.e., 4<sup>th</sup>-order dispersion is neglected.) The measured standard deviation is 0.28 ps/nm-km, which corresponds to a relative error of 1.6%. When multiplied by the length of the fiber, this translates into a standard deviation of 0.00011 ps/nm.

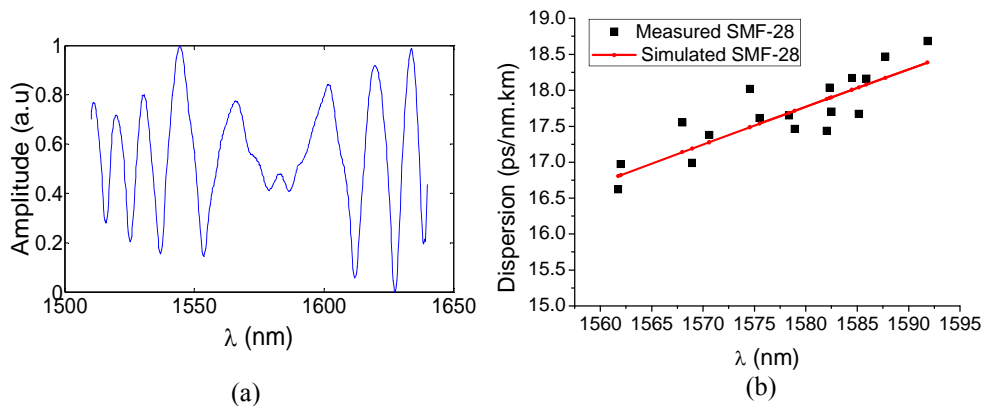


Fig. 4. (a) Experimentally obtained spectral envelope for a 39.5cm SMF-28 fiber. (b) Measured dispersion compared to published dispersion [27] for the same fiber.

A comparison between the measured and simulated interference patterns for SMF-28 is shown in Fig. 4(b). The slope of the measured dispersion closely matches that of the theoretical dispersion curve.

#### 4.2 Dispersion Compensating Fiber (DCF)

As a second method of verification, we measured dispersion on a short piece of DCF, whose dispersion value is approximately one order of magnitude higher than that of SMF28<sup>TM</sup>, and has an opposite sign. We used a 15.5 cm piece of DCF fiber, and the measurement results are given in Fig. 5. To verify the accuracy of our measurement, we also measured dispersion on an identical 100-m DCF using a commercial dispersion measurement system (Agilent 86038A), which employs the MPS technique. Again, our measured dispersion values are in good agreement with those measured by the commercial device, though the fiber length we used is almost 3-orders of magnitude smaller.

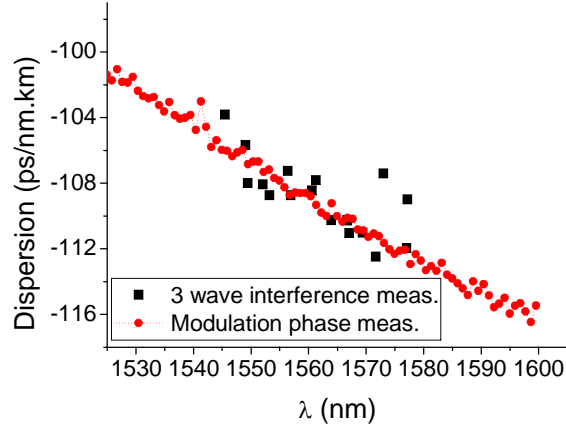


Fig. 5. Comparison of dispersion values measured by two methods. The red points are obtained on a 100-m-long DCF using the Agilent 83427A Chromatic Dispersion Measurement System. The black points are obtained on a 15.5cm DCF using the SAI.

The standard deviation of the measured data (with reference to a linear fit) using the SAI is 0.99 ps/nm-km, which corresponds to a relative error of 0.9%. When multiplied by the length of the fiber, this translates into a standard deviation of 0.00015 ps/nm.

#### 4.3 Twin-Hole Fiber (THF)

THF has been used for fiber poling to facilitate parametric generation in fibers [28, 29] or making fiber-based electro-optic switching devices [30]. In such nonlinear applications, dispersion of the fiber is an important parameter to be determined. However, dispersion property of the THF has never been reported, partly due to the lack of uniform THF over a large length. The fiber has a 3- $\mu$ m-diameter core and a numerical aperture that is higher than that of SMF28<sup>TM</sup>. The core is Ge-doped silica, and has an index similar to that of SMF28<sup>TM</sup>. Therefore, we expect the dispersion of THF to be slightly lower than that of SMF. We chose a THF length of 45 cm, and our measurement results are shown in Fig. 6. The standard deviation of the measured data (with reference to the linear fit) is 0.375 ps/nm-km, which corresponds to a relative error of 2.9%. Multiplied by the fiber length, this translates into a standard deviation of 0.00017 ps/nm. The slightly larger standard deviation compared to those for the SMF and DCF measurement is due to the higher loss in fiber coupling between the SMF and the THF, and hence the lower and more noisy signal level during the THF measurement.

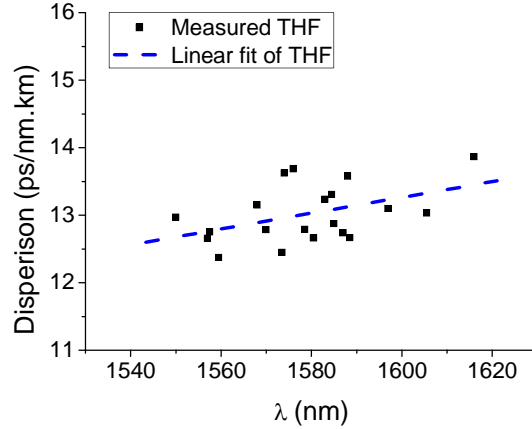


Fig. 6. Dispersion measured using a 45-cm long Twin Hole Fiber

## 5. Conclusion

In this paper we presented a novel fiber-based SAI to measure directly the dispersion parameters in short lengths of fiber ( $< 50$  cm), achieving a standard deviation as low as 0.0001 ps/nm without any curve fitting. The technique utilizes the spectral interferogram created by three reflections and extracts the second-order dispersion from the envelope of the interferogram. The technique is shown to be a simpler alternative to the Michelson or Mach-Zehnder interferometers. By eliminating one of the interferometer arms, the technique does not require calibration and is less susceptible to polarization and phase fluctuations. The constraints on the operating parameters of this technique, such as wavelength resolution, fiber length, and measurable bandwidth, were discussed in detail. This method can in general be used to measure the dispersion of any waveguide and is not limited to optical fiber.

We verified the technique experimentally by performing dispersion measurements on SMF28<sup>TM</sup> fiber and DCF samples. Our measurement results on the SMF28<sup>TM</sup> fiber showed good agreement with the simulated dispersion values based on published fiber geometry and material properties. Our measurement results on DCF agreed well with the measurement performed on a much longer DCF using a commercial dispersion measurement system. In addition to SMF28<sup>TM</sup> and DCF, single arm interferometry was used to measure the dispersion parameter of a twin-hole fiber for the first time.

## Acknowledgement

We thank Prof. Kazansky for providing the twin hole fiber samples, and we thank MPB Communications, Natural Science and Engineering Research Council of Canada, Ontario Centres of Excellence, and Premier's Research Excellence Award for their financial support.